Microscopic Origin of the Giant Ferroelectric Polarization in Tetragonal-like BiFeO$_3$

J. X. Zhang,[1,*] Q. He,[1,2] M. Trassin,[1] W. Luo,[1,3] D. Yi,[4] M. D. Rossell,[5] P. Yu,[1] L. You,[6] C. H. Wang,[7]
C. Y. Kuo,[8] J. T. Heron,[4] Z. Hu,[9] R. J. Zeches,[4] H. J. Lin,[8] A. Tanaka,[10] C. T. Chen,[8] L. H. Tjeng,[9]
Y.-H. Chu,[1,4,7] and R. Ramesh[1,4]

[1]*Department of Physics, University of California, Berkeley, California 94720, USA*
[2]*Advanced Light Source, Lawrence Berkeley National Laboratory, Berkeley, California 94720, USA*
[3]*Geballe Laboratory for Advanced Materials, Stanford University, Stanford, California 94305, USA*
[4]*Department of Materials Science and Engineering, University of California, Berkeley, California 94720, USA*
[5]*Department of Materials, ETH Zurich, Zurich, 8093, Switzerland*
[6]*Department of Electronic Engineering and Computer Science, University of California, Berkeley, California 94720, USA*
[7]*Department of Materials Science and Engineering, National Chiao Tung University, HsinChu 30010, Taiwan*
[8]*National Synchrotron Radiation Research Center, HsinChu 30077, Taiwan*
[9]*Max Planck Institute for Chemical Physics of Solids, Nöthnitzerstr. 40, 01187 Dresden, Germany*
[10]*Department of Quantum Matter, ADSM, Hiroshima University, Higashi-Hiroshima 739-8530, Japan*

We report direct experimental evidence for a room-temperature, ~ 130 μC/cm^2 ferroelectric polarization from the tetragonal-like BiFeO$_3$ phase. The physical origin of this remarkable enhancement of ferroelectric polarization has been investigated by a combination of x-ray absorption spectroscopy, scanning transmission electron microscopy, and first principles calculations. A large strain-induced Fe-ion displacement relative to the oxygen octahedra, combined with the contribution of Bi 6s lone pair electrons, is the mechanism driving the large ferroelectric polarization in this tetragonal-like phase.

The exploration of lead-free ferroelectrics with large polarization has been accelerated due to the demand for environmental-friendly materials. BiFeO$_3$ (BFO) single crystals and thin films show a large ferroelectric polarization of ~ 100 μC/cm^2 in its ground state (rhombohedral phase) [1–3], suggesting that BFO is one of the most promising candidates for lead-free piezo- or ferroelectric applications [4,5]. The ability to epitaxially tailor the ground state of materials has been a tool used to induce or enhance novel functionalities (e.g., ferroelectricity) [6–11]. The effects of epitaxial strain on the ferroelectric polarization of BFO films have been theoretically [12] and experimentally examined [13]. For BFO films under a compressive strain of up to 2%, a remnant polarization rotation has been observed; however, the intrinsic magnitude of the net polarization remains constant [12,14,15].

Recently, a tetragonal-like phase with a large c/a ratio of ~ 1.24 can be stabilized by utilizing highly mismatched substrates such as LaAlO$_3$ (LAO) to impose a large compressive epitaxial strain ($\sim 4.5\%$) to BFO [16–19]. This leads to a dramatic structural change of BFO from a rhombohedral-like (R) phase to a tetragonal-like (T) phase. Theoretical calculations have predicted a giant spontaneous polarization of up to ~ 150 μC/cm^2 in this new phase [12,20,21]. However, in a recent experimental study [17], a lower value of the spontaneous polarization (75 μC/cm^2) was reported in Mn-doped T-phase BFO and the theoretical predictions were questioned. The competition between polar instabilities and the antiferrodistortive rotations of

oxygen octahedra were suggested as the causes of the suppressed polarization.

In order to clarify the above ambiguity, we report direct measurements of the switched polarization in T-phase BFO. Saturated ferroelectric hysteresis loops from the mixed phase with a high concentration of T phase have been measured at room temperature, unveiling a spontaneous polarization of $\sim 130 \pm 5$ μC/cm^2. Using pulsed polarization measurements on samples with different volume ratios of T and R phases, we have been able to elicit a spontaneous polarization of ~ 150 μC/cm^2 in the pure T-phase BFO. The origin of this giant ferroelectric polarization has been studied by using a combination of first principles calculations, x-ray absorption techniques, and high-resolution scanning transmission electron microscopy (STEM).

Epitaxial BFO films with T phase, R phase, and mixed phases were grown on (001) LAO substrates by pulsed laser deposition. The ferroelectricity of these samples was studied by piezoresponse force microscopy (PFM). The detailed growth and PFM measurement conditions can be seen in the Supplemental Materials [22]. Figure 1(a) shows the out-of-plane PFM image after a box-in-box switching with a tip bias of ± 3 V in a pure T-phase BFO film. A clear domain pattern after switching indicates a robust ferroelectricity in this phase even in thicknesses down to ~ 7 nm. R- and mixed-phase films have been prepared as the control samples in order to explore the ferroelectricity in the T-phase BFO. Local piezoresponse phase loops were taken on the
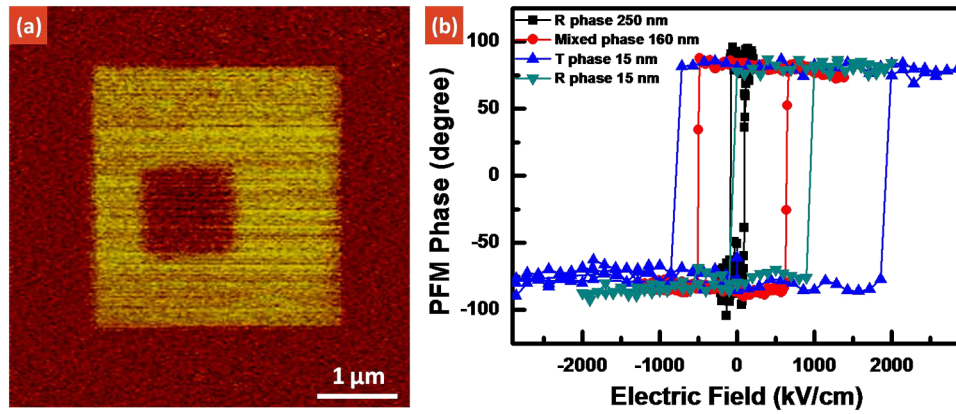
FIG. 1 (color online).   Local probe-based ferroelectric switching in T-phase BFO. (a) the out-of-plane PFM images after a positive ($+$ 3 V) and negative ($-$ 3 V) probe bias switching of the T-phase BFO; the relative dark and bright contrasts indicate the polarization states point upward and downward. (b) the piezoresponse phase curves of the pure T-phase (15 nm on LAO), mixed-phase ($\sim$ 160 nm on LAO), and R-phase BFO ($\sim$ 15 nm on SrTiO$_3$ and $\sim$250 nm on LAO).

T- ($\sim$ 15 nm thick on LAO), mixed- (160 nm thick on LAO), and R-phase ($\sim$ 15 nm on SrTiO$_3$ and $\sim$250 nm thick on LAO) films by applying an ac modulation and dc bias simultaneously on the PFM tip. Figure 1(b) shows sharp ferroelectric switching of all the T- (right-side-up triangles), mixed- (circles), and R-phase (squares and upside-down triangles) films, further confirming the remarkable ferroelectricity in T-phase BFO.

After proving the switchable polarization in the T-phase BFO, we now focus on answering the fundamental question: how large is the ferroelectric polarization in this phase? A direct experimental observation of a ferroelectric hysteresis loop from pure T-phase capacitors poses difficulty in films with thicknesses of less than 25 nm (the maximum thickness to stabilize pure T-phase BFO on LAO) due to a significant contribution from the leakage current. In order to extract the ferroelectric polarization in the pure T phase, we therefore measured the ferroelectric properties in mixed-phase samples with different mixture ratios, where the volume fraction of the T-phase BFO has been estimated using atomic force microscopy (AFM) and x-ray diffraction patterns (Supplemental Materials, Fig. S1 [22]). Figure 2(a) shows the high-resolution AFM image of a mixed-phase BFO with $\sim$70% T phase, where the flat area is pure T-phase BFO and the stripelike area is the T- and R-phase mixture. For macroscopic electrical characterization, a 50 nm-thick circular Pt top contact with a diameter of 24 μm was deposited by sputtering. A ferroelectric hysteresis loop (P-E loop) and pulsed measurements were performed using a RT6000 tester (Radiant Technologies, Inc). The P-E loops were acquired at room temperature and a frequency of 10 kHz. Figure 2(b) shows the typical P-E loops of the (001) oriented R- and mixed-phase samples measured at room temperature. A significant enhancement of remnant polarization in the mixed-phase BFO has been observed, $115 \pm 5 \ \mu$C/cm^2 (curved line with squares), compared to $60 \pm 5 \ \mu$C/cm^2 (curved line with circles)

observed in a (001) oriented R-phase BFO film. In order to extract the real ferroelectric properties, positive-up negative-down measurements [$\Delta P = P^*$ (switched polarization)-$\hat{P}$ (nonswitched polarization)] were carried out to confirm these values. The results are shown in Fig. 2(c) for the R- (squares) and the mixed-phase films with $\sim$70% (right-side-up triangles) and $\sim$90% (sideways triangles) volume fractions of the T-phase BFO. The mixed-phase samples show a high switched polarization of $\sim$230 and $\sim$270 μC/cm^2. Typically, the switched polarization value is approximately double the remnant polarization as measured from a quasistatic hysteresis loop. In contrast, the (001) oriented pure R-phase sample shows a switched polarization of $\sim$120 μC/cm^2, consistent with previous studies [3]. Figure 2(d) shows the volume-fraction-dependent switched polarization (ΔP) in BFO films. This plot suggests that the polarization increases in the mixed-phase films with the fraction of the T phase, which indicates that the enhancement of the polarization is mainly contributed from the T phase. A ΔP of $\sim$300 $\pm$ 20 μC/cm^2 in a pure T-phase BFO is obtained by a linear extrapolation.

In order to understand the microscopic origin of this large polarization in the T-phase BFO, soft x-ray absorption spectroscopy (XAS) assisted by theoretical simulations were used to investigate the detailed electronic structure of this phase. The XAS spectra were collected at the Dragon Beamline of the National Synchrotron Radiation Research Center in Hsinchu, Taiwan. With the photon energy scanned across the Fe $L_{2,3}$ absorption edges [23,24], linearly polarized x rays were shined to the BFO sample with the electric field (E) vector parallel or perpendicular to the c axis of the crystal [Fig. 3(a)]. The important conclusion from these spectra [Fig. 3(b)] is that there is a considerable polarization dependence: not only do the various peaks have different intensities, but also they show detectable energy shifts of several tenths of an eV. What we observe here is both "magnetic linear dichroism"
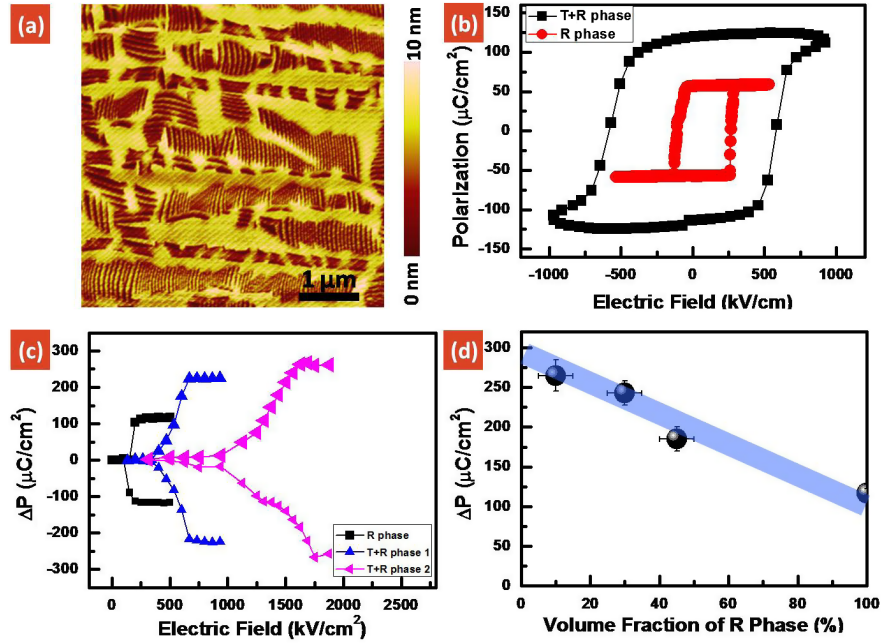
FIG. 2 (color online).   Macroscopic ferroelectric measurement of BFO films with different volume fractions of the *T* phase. (a) an AFM image of a mixed-phase film with a *T*-phase concentration of ~70%, where the flat area indicates the pure *T* phase and the stripelike area is the mixture of *T* and *R* phases. (b) room-temperature P-E loops of pure *R*-phase capacitor (circles) and mixed-phase capacitor (squares) with a *T*-phase concentration of ~70%; a strong enhancement of ferroelectric polarization contributed by the *T* phase in mixed-phase BFO has been observed. (c) pulsed measurement of the switched polarization of the *R* (squares) and mixed phases with the volume fraction of the *T* phase of ~70% (right-side-up triangles) and ~90% (sideways triangles). (d) switched polarization on the *R* and mixed phases as a function of the volume fraction of the *R*-phase BFO. A ferroelectric polarization of ~150 $\mu C/cm^2$ can be extrapolated in a pure *T*-phase capacitor according to this trend.

[25–29] and "crystal field dichroism" [29–31]. While the polarization dependence with respect to the magnetization axis shows up as variations in the peak intensities, crystal field dichroism gives also shifts in the peak positions.

The energy shift for the L_3 main peak is about 0.3 eV, while for the L_3 prepeak ($\sim$ 709 eV) it is about -0.4 eV in going from $E \parallel c$ to $E \perp c$. With the knowledge that the main peak is produced by transitions into the empty e_g-derived states and the prepeak to the empty t_{2g}, we can conclude that the $3z^2 - r^2$ orbital is likely be lower in energy than the $x^2 - y^2$, and that the xz/zy higher than the xy.

To understand the observed polarization dependence quantitatively, we have simulated the spectra using pure ionic crystal-field multiplet calculations [25] using the XTLS 8.3 code [24]. Starting from a set of parameters typical for an Fe^{3+} ion, we can find an optimal fit to the experimental spectra when we set the magnetic direction at 64° away from the *c* axis and use a splitting $\Delta e_g = E(x^2 - y^2) - E(3z^2 - r^2)$ of 0.35 eV and $\Delta t_{2g} = E(xy) - E(xz/yz)$ of -0.35 eV. The result is shown in Fig. 3(c). While the positive value for Δe_g is well within the expectations for the present case of compressive strain, the negative value for Δt_{2g} is rather counterintuitive. Next, we look into the origin of this level inversion.

To model the influence of the local coordination on the electronic structure in a physically tractable manner, we

now describe the potential at the Fe ion as an expansion of spherical harmonic functions:

$$V(r, \theta, \varphi) = \frac{4\pi}{2k + 1} \sum_{k=0}^{l} \sum_{m=-k}^{k} A_{k,m} r^k Y_k^m (\theta, \varphi)$$

in which the surrounding oxygen, bismuth, and iron ions contribute as point charges. Furthermore, we include explicitly the nearest-neighbor $O2p - Fe3d$ hybridization by using the phenomenological prescription developed by Harrison [32]. With these, we now can investigate how the displacements of the Fe and Bi ions from their high symmetry positions appear in the simulations of the spectra.

We start with the Fe ion placed in the center of the distorted octahedra with $c/a = 1.24$ as given by the crystal structure. This produces a positive, effective Δe_g and Δt_{2g}. To make Δt_{2g} negative, we must move the Fe ion along the *c* axis away from the center. We can find a reasonable fit to the experimental spectrum by setting $\Delta Z_{Fe} = 0.53$ Å as depicted in Fig. 3(d): the polarization dependence shows a negative energy shift for the prepeak and yet a positive shift for the main peak. Nevertheless, the shifts are not as large as experimentally observed [Fig. 3(b)]. Next, we include a displacement for the Bi ion with respect to the oxygen octahedra along the *c* axis. We are able to find the optimal solution when ΔZ_{Bi} is set at approximately 1 Å and ΔZ_{Fe} at
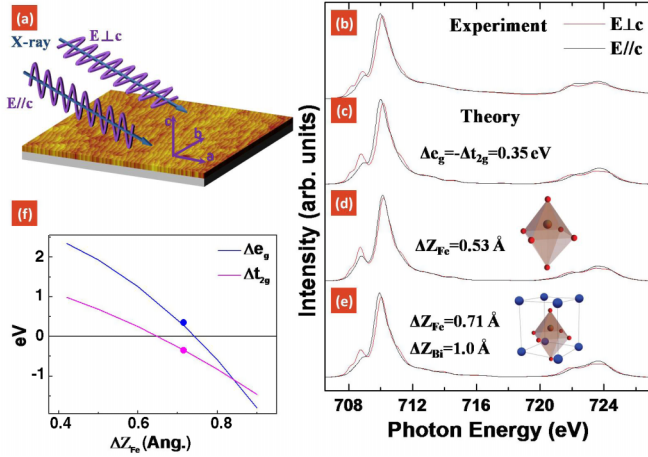
FIG. 3 (color online). Experimental and simulated x-ray absorption spectra showing the electronic structure of the T-phase BFO. (a) a linear polarized x ray shining on the T-phase BFO with E parallel and perpendicular to the c axis; (b) the experimental spectra; (c) the simulated spectra with $\Delta e_g = -\Delta t_{2g} = 0.35$ eV; (d) $\Delta Z_{Fe} = 0.53$ Å without applied electric field; (e) $\Delta Z_{Fe} = 0.71$ Å and $\Delta Z_{Bi} = 1$ Å with electric field, where the ΔZ denotes the movement of Fe away from the center (the cartoon is the cluster used in the simulation); and (f) the Δe_g (line with uppermost circle) and Δt_{2g} (line with lowermost circle) as functions of the ΔZ, where the ΔZ denotes the movement of Fe and Bi away from the oxygen center. The optimal values of Δe_g and Δt_{2g} are given by the lower and upper dots.

0.71 Å. Figure 3(e) shows that the experimental spectra have been reproduced quantitatively with both the correct polarization dependent intensity variations and energy shifts. As depicted in Fig. 3(f), the effective Δe_g (line with uppermost circle) and Δt_{2g} (line with lowermost circle) curves are plotted as the function of ΔZ_{Fe} with $\Delta Z_{Bi} \sim 1$ Å. Both Δe_g and Δt_{2g} values decrease with increasing ΔZ_{Fe}. Negative Δt_{2g} and positive Δe_g values can be found in the region of $\Delta Z_{Fe} = 0.65$–0.74 Å. The optimal values of Δe_g and Δt_{2g}, -0.35 eV and $+0.35$ eV, found by using the ionic analysis above, are given by the lower and upper dots.

In order to quantitatively investigate the ferroelectric contribution from Bi and Fe sites in the T-phase BFO, we have further performed first principles calculations of ferroelectric polarizations in both the T- and R-phase BFO. The details of the calculations are described in the Supplemental Materials [22]. The ferroelectric polarization is calculated by using the Berry phase method [33,34]. In the R-phase BFO, the ferroelectric polarization points along the pseudocubic [111] direction with $P_{[111]} = 92.5$ μC/cm^2. In the case of the T-phase BFO, the calculated structure corresponds to an in-plane compressive strain of 5% and a highly distorted lattice with $c/a = 1.26$, which is in excellent agreement with the experimental observation. The Fe sites become five-coordinated, as
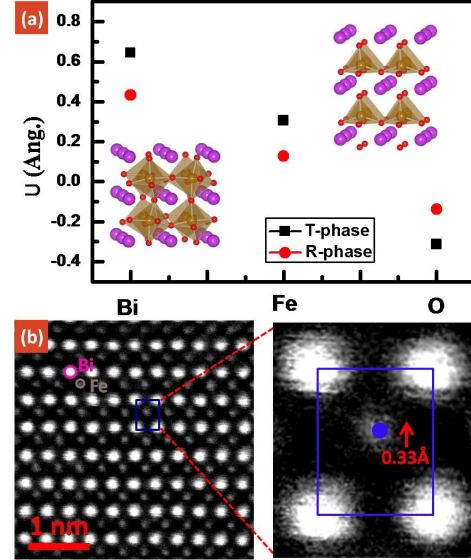

FIG. 4 (color online). First principles calculations and high-resolution STEM analysis of the T-phase BFO. (a) ferroelectric displacements of the Bi and Fe ions and the O octahedron in the R and T phases, obtained from first principles calculations. The displacements along the pseudocubic [111] direction are shown for the R phase, whereas, for the T phase, the displacements along the pseudocubic [001] direction are shown. The insert shows the crystal structures of the R- and T-phase BFO. (b) the high-resolution STEM image, giving a direct observation of the relative atomic displacement of Bi and Fe, which is consistent with the result from first principles calculations. 500 unit cells from different samples and locations have been analyzed in order to extract the average value of the atomic displacement shown in the magnified image.

shown in Fig. 4(a), in agreement with a previous theoretical study [18]. The ferroelectric polarization rotates from the [111] direction in the R-phase BFO to nearly the [001] direction in this T-phase BFO with $P_{[001]} = 145$ μC/cm^2.

We have employed a linearized approximation to separate the ferroelectric polarization into ionic contributions due to off-centering of Bi and Fe ions from the O octahedron (averaged position of the oxygen sites). Here, we focus on the [001] component of ferroelectric polarization in the T-phase BFO and the ferroelectric polarization in the [111] direction of the R-phase BFO. The corresponding ferroelectric displacements of Bi and Fe ions and the O octahedron from their nonpolar positions are plotted in Fig. 4(a). The key feature is that the Fe-O off-centering is enhanced in the T phase, compared to the one in the R phase.

From the projected density of states of the Fe minority-spin states, which are unoccupied states above the Fermi level, we obtain the crystal field splitting as $\Delta t_{2g} = -0.34$ eV and $\Delta e_g = 0.47$ eV (Supplemental Materials, Fig. S2 [22]). The Bi-O and Fe-O displacements of the T-phase BFO along the [001] direction are 0.95 Å and 0.62 Å, respectively. The density functional theory

calculations and the XAS analysis have a good agreement, in view of the simplicity of the semiempirical models used in the multiplet calculations and also the fact that the information extracted from the XAS experiments is (strictly speaking) only valid in the presence of the $2p$ core hole, while the density functional theory calculations have no core hole effect.

We have also calculated the Born effective charge tensor to obtain the relevant components for both phases. In a linearized approximation using the calculated Born effective charge tensor components of both phases and the respective ferroelectric displacements of the Bi, Fe, and O sites, the polarizations in the R and T phases are estimated as $P_{[111]} = 88$ μC/cm^2 and $P_{[001]} = 135$ μC/cm^2, respectively. These values are in good agreement with results obtained from Berry phase method. We then proceeded to calculate the respective contribution from off-centering of Bi-O and Fe-O to the ferroelectric polarization by using the Born effective charge tensor components and the ferroelectric displacements shown in Fig. 4(a). For the R-phase BFO, the Bi-O and Fe-O contributions along the [111] directions are 66 and 22 μC/cm^2; for the T-phase BFO, the Bi-O and Fe-O contributions along the [001] directions are 80 and 55 μC/cm^2. The Fe-O off-centering (along the [001] direction) in the T phase is more than twice that (along the [111] direction) in the R phase, which contributes to the large ferroelectric polarization in the T-phase BFO.

Further, the calculated atomic displacement between Fe and Bi ions has been evidenced by high-resolution STEM. The imaging conditions can be seen in the Supplemental Materials [22]. A representative image for a T-phase BFO film was taken along the [010] zone axis shown in Fig. 4(b). Such unprocessed images can be directly interpreted in terms of the projection of the atomic columns [35]. Analysis of this image enables us to determine the lattice parameters in the plane of the image ([100] and [001]). The in-plane and out-of-plane lattice parameters are ~ 3.75 Å and ~ 4.65 Å. We have also extracted the relative displacement (~ 0.33 Å along the [001] direction) between the Fe and the Bi ions by quantitative analysis of the STEM data [right panel in Fig. 4(b)], which shows a good agreement with both the XAS results and first principles calculations.

In summary, our room-temperature experiments provide direct evidence to reveal a giant polarization in T-phase BFO perovskite. Furthermore, the microscopic origin of ferroelectric polarization in the T phase has been studied with a combination of the XAS, first principles calculations, and STEM analysis. The giant polarization is attributed from both the large Fe-ion displacement relative to the negative charge center and the Bi $6s$ lone pair electrons. Such a result suggests that a large B-site-driven ferroelectric polarization can be induced by the epitaxial strain in BFO and opens pathways to search new ferroelectrics.

---

*To whom all correspondence should be addressed.
jinxing@berkeley.edu

[1] J. B. Neaton *et al.*, Phys. Rev. B **71**, 014113 (2005).
[2] D. Lebeugle *et al.*, Appl. Phys. Lett. **91**, 022907 (2007).
[3] Y.-H. Chu *et al.*, Mater. Today **10**, 16 (2007).
[4] F. Kubel and H. Schmidt, Acta Crystallogr. Sect. B **46**, 698 (1990).
[5] J. X. Zhang *et al.*, Nature Nanotech. **6**, 98 (2011).
[6] J. H. Lee and Karin M. Rabe, Phys. Rev. Lett. **104**, 207204 (2010).
[7] M. Ieong *et al.*, Science **306**, 2057 (2004).
[8] J.-P. Locquet *et al.*, Nature (London) **394**, 453 (1998).
[9] M. P. Warusawithana *et al.*, Science **324**, 367 (2009).
[10] J. H. Haeni *et al.*, Nature (London) **430**, 758 (2004).
[11] H. N. Lee *et al.*, Nature (London) **433**, 395 (2005).
[12] C. Ederer and N. A. Spaldin, Phys. Rev. Lett. **95**, 257601 (2005).
[13] J. Wang *et al.*, Science **299**, 1719 (2003).
[14] D. H. Kim *et al.*, Appl. Phys. Lett. **92**, 012911 (2008).
[15] H. W. Jang *et al.*, Phys. Rev. Lett. **101**, 107602 (2008).
[16] Z. Chen *et al.*, Appl. Phys. Lett. **96**, 252903 (2010).
[17] H. Bea *et al.*, Phys. Rev. Lett. **102**, 217603 (2009).
[18] D. Mazumdar *et al.*, Nano Lett. **10**, 2555 (2010).
[19] M. N. Iliev *et al.*, Phys. Rev. B **82**, 014107 (2010).
[20] A. J. Hatt *et al.*, Phys. Rev. B **81**, 054109 (2010).
[21] D. Ricinschi *et al.*, J. Phys. Condens. Matter **18**, L97 (2006).
[22] See Supplemental Material http://link.aps.org/supplemental/10.1103/PhysRevLett.107.147602 for the detailed growth, characterizations, and calculations.
[23] Q. He *et al.*, Nature Commun. **2**, 225 (2011).
[24] A. Tanaka and T. Jo, J. Phys. Soc. Jpn. **63**, 2788 (1994).
[25] P. Kuiper *et al.*, Phys. Rev. Lett. **70**, 1549 (1993).
[26] F. Nolting *et al.*, Nature (London) **405**, 767 (2000).
[27] D. Alders *et al.*, Phys. Rev. B **57**, 11623 (1998).
[28] E. Arenholz *et al.*, Phys. Rev. B **74**, 094407 (2006).
[29] S. I. Cziszar *et al.*, Phys. Rev. Lett. **95**, 187205 (2005).
[30] N. Hollmann *et al.*, Phys. Rev. B **82**, 184429 (2010).
[31] M. W. Haverkort *et al.*, Phys. Rev. B **69**, 020408(R) (2004).
[32] W. A. Harrison, *Electronic Structure and the Properties of Solids* (Dover, New York, 1989).
[33] R. Resta, Ferroelectrics **136**, 51 (1992).
[34] R. D. King-Smith and D. Vanderbilt, Phys. Rev. B **47**, 1651 (1993).
[35] R. Erni *et al.*, Phys. Rev. Lett. **102**, 096101 (2009).